

We are IntechOpen, the world's leading publisher of Open Access books Built by scientists, for scientists

6,900

Open access books available

186,000

International authors and editors

200M

Downloads

Our authors are among the

154

Countries delivered to

TOP 1%

most cited scientists

12.2%

Contributors from top 500 universities



WEB OF SCIENCE™

Selection of our books indexed in the Book Citation Index
in Web of Science™ Core Collection (BKCI)

Interested in publishing with us?
Contact book.department@intechopen.com

Numbers displayed above are based on latest data collected.
For more information visit www.intechopen.com



Review of Autonomous Underwater Vehicles

Kondeti Lakshmi Vasudev

Additional information is available at the end of the chapter

<http://dx.doi.org/10.5772/intechopen.81217>

Abstract

The exploration of ocean space requires underwater vehicles (UV) such as submarines, autonomous underwater vehicles (AUV), manned underwater vehicles, remotely operated vehicles (ROV) and ship towed instrumentation packages. Of these, AUVs dominate the exploration of deep oceans. The list of applications where UVs can be employed include long-term deployments where they would serve as platforms for spatiotemporal samplings of physical characteristics (e.g., temperature, depth, conductivity, current) of the water column; use of multiple vehicles for mapping out an evolving phenomenon such as hydrothermal vents, tsunamis, etc., rapidly; transiting long distances to a site for making observations as part of a response team; search and mapping of seabed minerals; underwater warfare using submarines; and mine hunting, pipe laying, and inspection and maintenance of offshore structures.

Keywords: computational fluid dynamics, autonomous underwater vehicles, hydrodynamic drag, wake fraction

1. Introduction

UVs can be classified in a variety of ways. Submarines are manned underwater vehicles. Their operating speed varies from 8 to 20 m/s and depth of operation varies from 200 to 600 m. The length of submarines in existence varies from 57.3 m (Dolphin 1 class) to 175 m (Typhoon class). Submarines are used in underwater warfare, covert operations, and coastal defense. AUVs are underwater robots with operational speeds varying from 0.5 to 2 m/s, and a depth of operation varying from 200 to 6000 m. The length of AUVs varies from 1.42 m (AUV Cormoran) to 10 m (AUV Urashima). They mostly have torpedo shaped hull forms. AUVs can be employed to collect data samples of physical characteristics of water such as temperature, salinity, density, depth and conductivity and map out hydrothermal vents, tsunamis etc. AUGs are underwater robots which can hold their positions by gliding against the current or waves

by making themselves neutrally buoyant and drift with the currents and waves or rest on the sea bed. They do not require thrusters or propellers for propulsion. AUGs are capable of carrying out a mission economically in comparison to AUVs and have much larger endurance. Few existing AUGs even have the capability to derive their propulsive energy from the ocean itself. One concept is to use the temperature differences in the ocean thermocline (principle of thermal stratification to convert heat into mechanical energy). In general, these vehicles are very small in size. Their operating speed varies from 0.1 to 0.5 m/s.

Towed fish are torpedo shaped bodies without any active propulsion. They are towed by a ship by a mooring line and have limitations on the depth of operation. Their depth of operation is usually limited to about 200 m. Typically, they carry instruments such as acoustic Doppler current profiler, DRAKE (Depth and Roll Adjustable Kite for Energy flux measurements) etc. During their deployment, the ship speed is typically in the range of 2.5–5.5 m/s. ROVs are tethered vehicles whose mission plan is executed from onboard a ship. They are often linked to the ship by either a neutrally buoyant tether or a load carrying umbilical cable. Their depth of operation varies from 200 to 11,000 m. They can be employed in exploration and mapping of seabed minerals.

Unlike ROVs, deep submergence vehicles (DSV), autonomous surface vehicles (ASV) and AUGs are unmanned submersibles without tethers or umbilical cables and follow a predefined path without operator intervention. They usually carry the power source onboard in the form of batteries and have a payload in accordance with their mission. The power supply unit and the speed details of few existing AUVs are given in **Table 1**.

Even though the initial interest in AUVs was developed for oceanographic research in the late 1960s by the University of Washington using Special Purpose Underwater Research Vehicle

AUV	Speed (knots)	Endurance (km or h)	Energy storage/supply device
ARCS (Canada)	5.5 (max.) 4 (cruising)	36 km (1 Ni-Cd battery) 72 km—2 Ni-Cd 235 km—Al-O ₂	1 or 2 Ni-Cd battery (10 kW-h. each) or Al-O ₂ fuel cells (100 kW-h)
AURORA (Canada)	3.5 (max.) 1.5-2 (Cruising)	750 km	Li ion battery units
THESEUS (Canada)	4 (Cruising)	780 km	Ag-Zn battery units (360 kW-h)
HUGIN 3000 (Norway)	4 (Cruising)	6–8 h—Ni-Cd 36 h—Al-O ₂	Ni-Cd battery units (3 kW-h) Al-O ₂ semi-fuel cells (18 kW-h)
DeepC (Germany)	6 (max.) 0.5-4 (Cruising)	400 km 60 h	PEM fuel cells
AUTOSUB (UK)	2-4 (Cruising)	500 km 144 h	Alkaline primary battery units
OKPO 6000 (Korea)	3 (max.)	10 h	Ag - Zn battery units
MARIDAN 600 (Denmark)	4 (max.) 3 (Cruising)	36 km 10 h	Pb-H ₂ SO ₄ battery units
CETUS (US)	5 (max.) 1.5-2.5 (Cruising)	20-40 km	Pb-H ₂ SO ₄ battery units

AUV	Speed (knots)	Endurance (km or h)	Energy storage/supply device
REMUS (US)	5 (max.) 3 (Cruising)	46.3 km	Pb-H ₂ SO ₄ battery units (400 kW-h)
AQUA EXPLORER 2 (Japan)	2 (max.) 1 (Cruising)	24 hrs	Li primary battery units (3870 W-h)
R-One Robot (Japan)	3.6 (max.) 2 (Cruising)	120 km 25 hrs	CCDE (60 kW-h)

Table 1. General characteristics of AUVs around the world (from Thomas, 2003).

(SPURV) (see **Figure 1(a)**), it is only recently AUVs are being actually used in oceanographic research. Few recent instances where AUVs and ROVs are employed are: the Autonomous Benthic Explorer (ABE) (see **Figure 1(b)**) deployed in 1996-1997 in the Juan de Fuca region off the coast of Oregon to map the magnetic characteristics of a new lava flow; Odyssey IIB (see **Figure 1(c)**) class vehicles from MIT employed to study the convective overturning associated with the mixing of fresh and salt water in the Haro Strait on the US-Canadian northwest border; Woods Hole Oceanographic Institute's Argo ROV (see **Figure 1(d)**) played a major role in the 1985 discovery of the wreck of the RMS Titanic and German battleship Bismarck; and OKPO-6000 (see **Figure 1(e)**) explored successfully 2300 m deep seabed in 1996 near the Dok-Do island in the East Sea of Korea. Few other examples of the present day AUVs are Japan's AUV Urashima (see **Figure 1(f)**), which is a torpedo-shaped vehicle with depth rating up to 3500 m and whose hull frames are made of titanium; Norway's HUGIN 3000 (see **Figure 1(g)**) is a tail boomed vehicle that can operate in 3000 m depth; Canadian AUV Theseus (see **Figure 1(h)**), which is a torpedo-shaped vehicle of length 10.7 m, diameter 0.127 m and depth of operation of to 1000 m; UK's AUV Autosub (see **Figure 1(i)**), which is also a torpedo-shaped vehicle with depth rating of 6000 m, endurance of 4400 hrs and with a hull made of titanium; Denmark's Atlas Maridan Seaotter Mk II (see **Figure 1(j)**), which is a modular flat fish design with a length of 3.65 m and depth of operation 600 m; AUG Seaglider (see **Figure 1(k)**) which is a tear drop shaped vehicle of length 1.8–2 m depending on the configuration and Indian AUV Maya (see **Figure 1(l)**) which is a torpedo-shaped vehicle that is 1.72 m long and 0.234 m in diameter.

1.1. DESIGN OF UVs

The design of UV is mission specific and each UV is unique in design because it needs to cater to its unique set of mission requirements. However, the design objectives related to their underwater usage are based on hydrodynamic drag, power, propulsion, maneuvering and buoyancy control. Of these, the hydrodynamic drag is most important because it directly affects the power requirement, range, and endurance. Therefore, minimization of drag is a central objective in AUV design and it is an important problem in the area of marine hydrodynamics. This can be accomplished, in general, by some combination of (i) streamlined shaping of the hull, (ii) controlling boundary-layer, e.g., polymer injection or slot suction, (iii) energy-saving propulsion; e.g., a wake adapted propeller or a suction slot with a stern jet, and (iv) efficient maneuvering consistent with hydrodynamic stability. The first two of this list



Figure 1. Diverse forms of AUVs. (a) AUV SPURV [2], (b) Autonomous Benthic Explorer [3], (c) AUV Odyssey IIB [4], (d) ROV Argo [5], (e) AUV OKPO 6000 [6], (f) AUV Urashima [7], (g) AUV Hugin 3000 [8], (h) AUV Theseus [9], (i) AUV Autosub [10], (j) AUV Atlas Maridan 300 [11], (k) AUG Seaglider [12], (l) AUV Maya [13].

attempt to reduce skin friction and pressure drag while the third attempts to extract energy lost to the fluid surrounding the vehicle. A complete systems design must simultaneously take into account all these four aspects though the complex nature of the complete problem does not permit analytical systems design approach [1].

For propelled vehicles, a body that has minimum drag need not be the one that requires minimum power because the benefit from the reduction in drag may be lost because of poor wake fraction which implies poor propulsive efficiency of the propeller which is fitted in the vehicle's wake. The efficiency of the propeller located in the wake of the hull is in general inversely proportional to the wake fraction and also to the thrust deduction factor. In order to optimize hull shapes of UVs, both drag (minimization) and wake fraction (minimization) should be considered simultaneously.

At present, the UV design process is mainly dominated by ad-hoc approaches that either use design experience or rely on simple rules of thumb [2] based on empirical formulations of hydrodynamic drag and wake fraction. Although an empirical approach is convenient at the preliminary design stage, it does not consider the local fairing effects on the flow, which play an important role in the estimation of drag and wake fraction. To overcome these limitations, the experimental approach using model testing in towing tank is often used, which, however, is both time consuming and expensive and, as a result, cannot be done for many designs. Typically, a maximum of three designs can be tested in a towing tank, which is certainly not enough for establishing a near optimum design. In this regard, the recent advances in CFD can play an important role in the UV design because with CFD the local fairing effects and the variations of flow can be accurately predicted so that hydrodynamic evaluations of many designs are possible in a short time economically. As a result, a near optimum design can be obtained in principle if CFD approach is integrated into the design process. Use of CFD to analyze the flow field around the hull and to perform computations of viscous drag has found interesting applications in ship design [2–4].

Although CFD has the advantage of reducing the time and cost of each analysis, it is difficult to manually change the design parameters of the UV hull form and conduct each analysis to obtain an optimized shape. Hence, there is a requirement to solve the problem with a process of optimization which is robust and automatic. Such attempts have been made for ships [3, 4] with limited success. In recent years, multidisciplinary design optimization (MDO) methods are being increasingly and effectively used to identify optimal designs [2].

The optimization of hull shape of UVs therefore, will ideally involve simultaneous minimization of drag and wake fraction and maximization of volume subject to constraints on the parameter space. The methodology presented in this thesis seeks to establish such a capability wherein the optimization technique based on genetic algorithm (GA) and CFD solver are seamlessly integrated with the computer aided geometric design (CAGD) tool in a single code that requires no user intervention during the entire optimization process.

1.2. Literature review

A brief review of the literature is described in this section in chronological order.

Ref. [5] conducted experiments on a systematic series of 24 mathematically related streamlined bodies of revolution to measure drag force, Reynolds stresses, pressure, kinetic energy, axial and radial velocity profiles, stern and far wake at deep submergence. The body geometric parameters are fineness ratio, prismatic coefficient, nose radius, tail radius and the position

of the maximum section. The mathematically derived series of bodies of revolution, which was designated series 58, are used to form the offsets of the models using a sixth degree polynomial.

Ref. [6] conducted experiments on a 1:6 spheroid (MS) of 1.578 m long and 25 cm maximum diameter in a wind tunnel at a speed of 12 m/s and measured pressure distributions, mean velocity profiles, and Reynolds stresses in the thick axisymmetric turbulent boundary layer near the tail of the body. The thick boundary layer is characterized by significant variations in static pressure across it and very low level of turbulence. It is concluded that the static pressure variation is associated with a strong interaction between the boundary layer and the potential flow outside it, while the changes in the turbulence structure appear to be a consequence of the transverse surface curvature. The main conclusion was that by using the thin boundary layer calculation it is not possible to predict the behavior of the flow in the tail region of a body.

Ref. [1] introduced an automatic synthesis approach to minimum drag axisymmetric hull shapes in non-separating flow with constraints on volume and speed. The optimization was done in a finitely constrained parameter space with eight-parameter 'rounded-nose-tail boom' bodies. The parameters are the zero radius of curvature of the nose, maximum diameter and its axial location, curvatures at the locations of the maximum diameter and aft inflection point, radius and slope at the aft inflection point and the terminal radius of the profile. The drag was evaluated exploiting laminar flow by avoiding flow separation. Ref. [7] developed a multi-criteria optimization model for ship design which is a problem with multiple local optima with widely varying sets of designs. Simulated annealing had been successfully implemented to optimize the ship design process as a global optimization tool. The decision system was based on the analytic hierarchy process.

Ref. [8] discussed the Approximation Management Framework (AMF), for solving optimization problems which aims to use the cheaper low fidelity models in iterative procedures with occasional, but systematic, recourse to expensive high fidelity models. Three versions of AMF using nonlinear programming algorithms are implemented on a three dimensional (3D) aerodynamic wing and a two dimensional (2D) airfoil. The three methods discussed were augmented Lagrangian AMF, sequential quadratic programming AMF and AMF based on 'multilevel algorithm for large scale constrained trust-region optimization'.

Ref. [9] worked on implementing a downhill simplex method with constraints on volume displacement and transverse moment of area of water-plane of a ship to minimize its total drag. The parent hull form considered is classical Wigley hull of length 122 m defined by NURBS (Non-Uniform Rational B-Spline) surface. The ITTC formula is used to calculate the frictional drag and the wave drag was predicted using zeroth-order slender-ship approximation. Ref. [3] developed two simulation based ship design approaches, one of which is 'narrow band derivative-free' approach and the other is 'variable fidelity' approach. They used CFD to evaluate the objective function, which is the total drag of a ship, and validated the results by conducting model tests. Similar work was done by [10, 11].

Ref. [12] studied practical and quantitative methods for measuring effectiveness in naval ship design. A method is presented that uses the analytic hierarchy process combined with

multi-attribute value theory to build an overall measure of 'effectiveness' and 'overall measure of risk function' using trained expert opinion to replace complex analysis tools. Ref. [13] implemented topological optimization techniques to reduce the weight of the composite advanced sail structure. The approach is applied to reinforcement layout optimization under an asymmetric wave slap loading condition. A high complexity model in the form of multilayered shell and a low complexity model in the form of stiffened shell are developed for layout optimization. Ref. [14] developed a framework for design optimization for problems that involve two or more objectives which may be conflicting in nature. The framework is implemented for the design of space propulsion involving a response surface based multi-objective optimization of a radial turbine for a liquid rocket engine. The surrogate model is integrated with GA-based Pareto front construction and can be effective in supporting global sensitivity evaluations. It has been concluded that a global sensitivity analysis provided a summary of the effects of design variables on objective function analysis and it is determined that no variable could be eliminated from the analysis.

Ref. [15] developed an underwater glider ALEX with independently controllable main wings and conducted wind tunnel experiments. To establish a mathematical model of the glider CFD is used to estimate the hydrodynamic forces acting on it and the results were compared with the experiments. Ref. [16] implemented a simulated annealing technique for the shape optimization of Cormoran AUV operating at snorkeling depths with constraints on surface area and volume and validated the results by conducting experiments. The objective was to minimize the wave making resistance at snorkeling depths while using an empirical formula for the calculation of the viscous drag. Ref. [17] developed a design optimization process for AUV using GA with cost, effectiveness and risk as the main design objectives. The design parameters are diameter, length to diameter ratio, forward shape coefficient, aft shape coefficient, endurance, speed, communication, payload, propulsion, battery and electronics configurations, wall thickness and material.

Ref. [18] studied the drag and turbulent noises created by the equipment like sonar array, electronic devices, antennas and video cameras. Automatic multi-objective optimization is applied using 'design of experience' as well as GA. Ref. [19] developed a Multidisciplinary Design Optimization (MDO) approach to the design of submarine considering four objectives, namely, deck area, drag, structural design and maneuvering. Particle Swarm Optimization (PSO) technique is used. The length of the parallel middle body, maximum diameter, tail shape parameter and nose shape parameter are the design variables. Ref. [20] developed an AUV PICASSO (Plankton Investigatory Collaborating Autonomous Survey System Operon). To improve the overall propulsive performance and maneuverability numerical and experimental study has been carried out and concluded that by changing the fore and aft hull form propulsive performance has been improved.

Ref. [21] developed a hybrid driven underwater glider Petrel. CFD simulations were carried out to study the glide mode of the glider. The glide efficiency is found to be significantly influenced by the chord length of the wing, the stability of the vehicle is influenced by the sweep angle of the wing and the glide stability is influenced by the location of the wing. Ref. [22] developed the Flinders AUV. Shape optimization of the vehicle with a ducted

propeller has been carried out using CFD software. The Design of Experiments (DOE) method based single objective optimization problem with minimizing drag as the objective has been formulated and solved with location of the sail, the separation between sail and transponder and angle of attack of the nozzle as the variables. Ref. [23] developed an approach to characterize the spiraling motion of underwater gliders and applied on Seawing underwater glider. The hydrodynamic coefficients are computed using CFD. The proposed approach has been validated by conducting field experiments. Ref. [24] investigated hydrodynamic characteristics like drag and lift forces of the USM shallow underwater glider whose length is 1.3 m with 0.17 m diameter by using CFD.

2. Geometry definition of the hull forms

The geometry of the UV is axisymmetric and is shown in **Figure 2**. The parameterized shape of the body is given by [16]:

$$\begin{aligned}
 r(x) &= r_{\max} \left(1 - \left(\frac{L_n - x}{L_n} \right)^{n_n} \right)^{1/n_n} && \text{for } 0 \leq x \leq L_n \\
 r(x) &= r_{\max} && \text{for } L_n \leq x \leq L_n + L_m \\
 r(x) &= r_{\max} \left(1 - \left(\frac{x - L_n - L_m}{L_t} \right)^{n_t} \right) \text{ OR } r_{\max} + \frac{(x - L_n - L_m)(r_t - r_{\max})}{L_t} && \text{for } L_n + L_m \leq x \leq L_n + L_m + L_t \\
 L_n + L_m + L_t &= L
 \end{aligned} \tag{1}$$

where r_{\max} is the maximum radius of the body so that the maximum diameter is $d_{\max} (=2r_{\max})$ and a middle body length L_m has this radius, $r(x)$ is the variation of radius over the total length

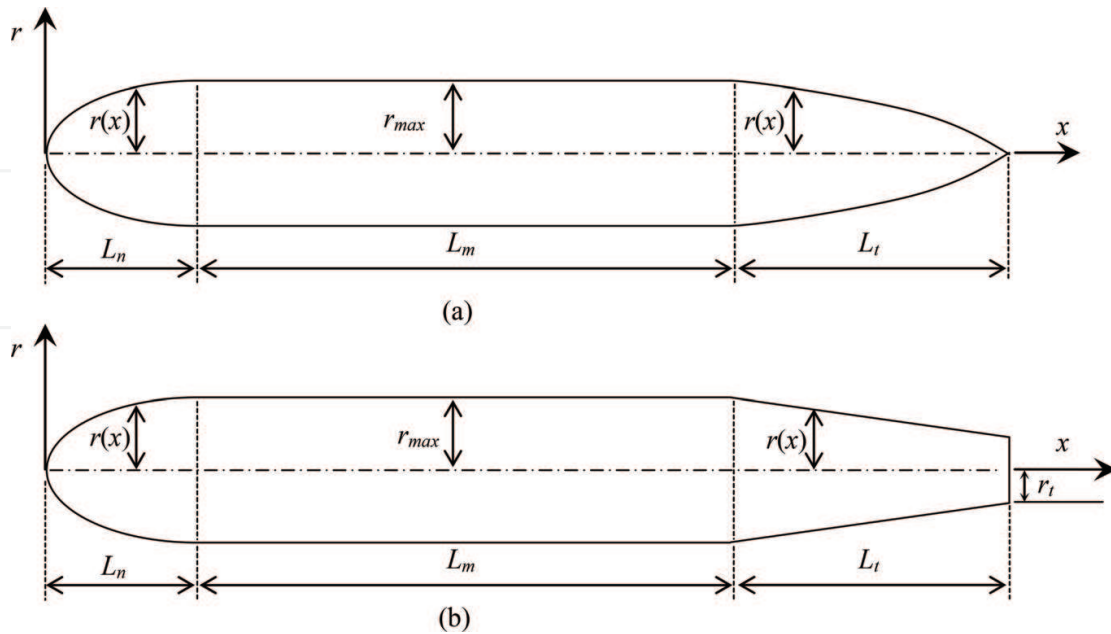


Figure 2. Parameterization of the hull geometry. (a) Axisymmetric body without blunt tail. (b) Axisymmetric body with blunt tail.

L_n , L_n and L_t are the lengths of the nose and the tail respectively and the exponents n_n and n_t are associated with the nose and tail shapes respectively.

The shape given by Eq. (1) leads to a conical nose shape (i.e. linear $r(x)$) for $n_n = 1$ and a conical tail shape for $n_t = 1$. For large values of n_n , the nose shape profile approaches a rectangle (i.e. $r(x)$ approaches r_{max}) and for large values of n_t , the tail shape profile also approaches a rectangle. For $n_n < 1$ and $n_t < 1$, the nose and tail shapes reverse the sign of their curvatures. The volume (∇), a design variable, is

$$\nabla = \pi \int_0^L r^2(x) dx \quad (2)$$

In this work, we have chosen two axisymmetric vehicles, namely, toy submarine USS Dallas (**Figure 3**) and AUV Cormoran (**Figure 4**). The parameters of these five vehicles are given in **Table 2**. It is to be noted that there is no parent hull form for the submarine. Its parameters, given in **Table 2**.

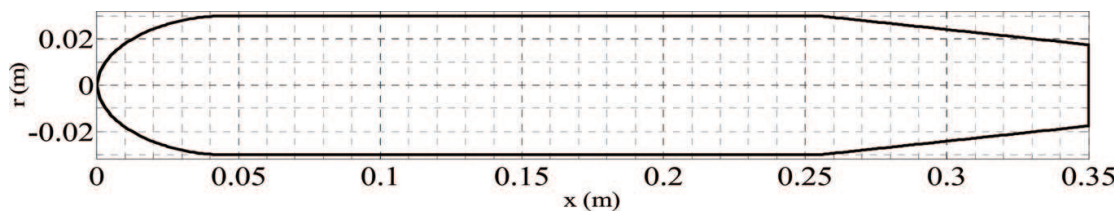


Figure 3. Toy submarine USS Dallas.

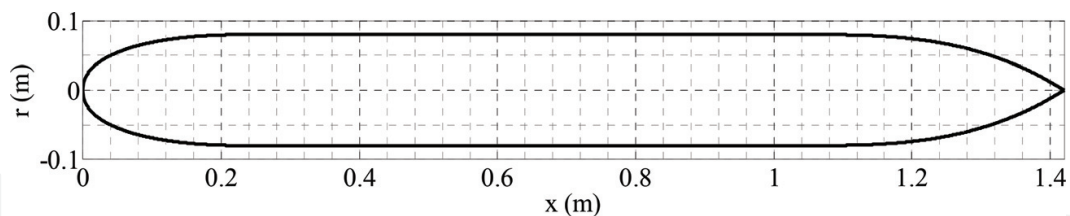


Figure 4. AUV Cormoran.

Parameters	Toy submarine USS Dallas	AUV Cormoran
Parameters of two hull shapes		
L_n (m)	0.045	0.24
L_m (m)	0.210	0.8
L_t (m)	0.095	0.38
L (m)	0.35	1.42
r_{max} (m)	0.03	0.08
r_t (m)	0.0175	0

Parameters	Toy submarine USS Dallas	AUV Cormoran
Parameters of two hull shapes		
n_n	1.9	2.3
n_t	1	3
l_s (m)	—	—
U (m/s)	0.5	1
S (m ²)	0.0612	0.63
∇ (m ³)	0.000848	0.0245
$L/2r_{max}$	5.8	8.875
$\nabla^{2/3} / S$	0.6795	0.134

Table 2. The hull parameters.

Toy submarine USS Dallas was studied by [2] who reported drag force obtained from CFD simulation for a speed of 0.5 m/s which translates to $Re_L = 1.75 \times 10^5$. AUV Cormoran was studied by [16] who reported drag coefficients for a few speeds measured in towing tank.

3. Computational domain and discretization

The computational domain is shown in **Figure 5** where S_B is the body boundary, S_{F1} is a surface enclosing the subdomain Ω_1 as well as S_B and S_F is a surface enclosing the entire domain Ω , which encloses Ω_1 . The domain Ω , bounded by S_F and marked ABCD in the x - z or the vertical plane (x - y or the horizontal plane being similar since the body is axisymmetric), has a length $6.2 L$ (L being the length of the body) and a height (i.e. breadth in the z direction) of $1.2 L$. The domain length upstream is $0.7 L$ and the domain length downstream is $4.5 L$. The domain is large enough to capture the entire viscous-inviscid interaction and the wake development. It should be noted that the domain Ω embeds in it the domain Ω_1 as well as the body surface S_B . The mesh of the domain Ω is modeled by a uniform grid such that on the boundaries AB and CD, the number of cells is N_z ($=N_y$) and on the boundaries AD and BC, the number of cells is N_x . Thus, the domain Ω has a grid of $N_x \times N_y \times N_z$ cells in x (length), y (breadth) and z (height) directions of the cuboid Ω .

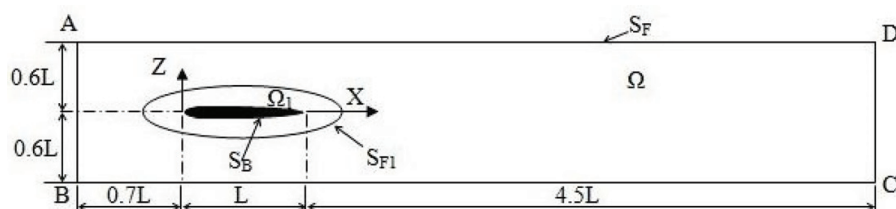


Figure 5. Fluid domain and boundaries for CFD calculations of AUV Cormoran, Afterbody 1 and AUV Autosub.

The subdomain Ω_1 is defined such that a point on S_{F1} is at a (perpendicular) distance of l from S_B and is meshed with N_r cells over this distance l with a graded mesh. The grid point nearest to S_B (wall adjacent cell size) is located at a (perpendicular) distance of l_1 from it and a successive ratio (g), defined as the ratio of successive distances between grid points normal to the body surface, is prescribed. This ensures that

$$l = \sum_{i=1}^{N_r} l_1 g^{i-1} \quad (3)$$

and the mesh over Ω_1 is an H-type structured mesh.

The successive or growth ratio (g) should be so chosen that it prevents the wall adjacent cells from being placed in the buffer layer of $y^+ = 1$. The acceptable distance between the cell centroid and the wall adjacent cells is usually measured in the wall unit y^+ . However, it requires some trial and error to determine a suitable value of l_1 . In all calculations, a value of $l_1 = 0.001$ mm was adopted which is found to satisfy the $y^+ < 1$ requirement. The mesh of the domain Ω_1 , which embeds the body, was modeled by adopting $g = 1.1$ and a grid of $N_x \times N_r \times N_\theta$ cells in longitudinal, radial and circumferential direction respectively. The interface between Ω_1 and Ω is handled by the CFD solver by constructing interfacial cells.

3.1. Boundary conditions

The conditions imposed on boundaries of the fluid domain (see **Figure 5**) are:

- a. At the inlet boundary AB, velocity U normal to the boundary is specified.
- b. On the boundary CD, the pressure outlet boundary condition has been imposed. It implies that the pressure (p) is set to gauge pressure (i.e. $p = 0$) and the gradients of k and ω are set to zero.
- c. On the top boundaries AD, BC ($z = \pm 0.6 L$) and the two side boundaries ($y = \pm 0.6 L$), the zero shear stress condition has been imposed.
- d. On the surface boundary S_B , the no slip condition is specified.

3.2. Solver parameters

The commercial CFD solver has been used and the solver parameters are presented in **Table 3**. The velocity components are governed by the momentum equations. The Roe flux algorithm is used for coupling the pressure and velocity terms. Second order upwind scheme is adopted for the discretization of pressure, momentum, turbulent kinetic energy and turbulence dissipation rate. The convergence criterion of 10^{-4} is set for velocity components and 10^{-6} for continuity, k and ω . The termination of the program is based on the final steady value of drag. All simulations were run using 3D steady segregated RANS solver. In all the optimization problems treated in this thesis, the number of iterations was fixed at 2000, and the drag force has been obtained by its average over one cycle (between a peak and a trough) preceding the last iteration number.

Discretization	
Pressure	Body force weighted
Momentum; turbulent kinetic energy and dissipation rate	Second order upwind
Fluid properties	
Density (ρ)	1000 kg/m ³
Kinematic viscosity (ν)	10 ⁻⁶ m ² /s
Roughness parameters	
Roughness constant (C_S)	0.5
Roughness height (K_S)	0
Turbulence criteria at inlet	
Turbulent intensity (T)	5%
Turbulent length scale (l_T)	0.001 L
Under relaxation factors	
Pressure	0.3
Density	1
Body forces	1
Momentum	0.7
Turbulent viscosity	1
Turbulent kinetic energy	0.8
Turbulent dissipation rate	0.8

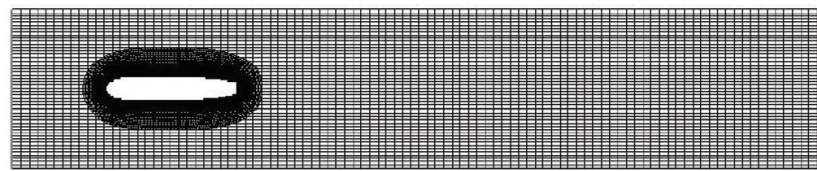
Table 3. Solver parameters and constants used in the study.

This reduces the computational effort significantly because instead of about 4000–6000 iterations for an accurately converged value of drag, one can use only 2000 iterations for all intermediate configurations during the optimization process. The drag of the final optimized configuration, however, is obtained by approximately 4000–6000 iterations for high accuracy.

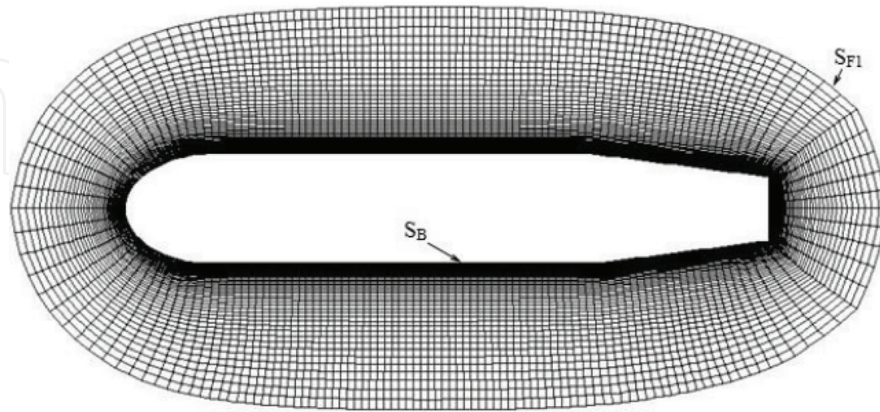
4. CFD analysis of toy submarine USS Dallas

The mesh of the domain Ω (see **Figure 5**) for toy submarine USS Dallas has 260,100 cells ($=N_x \times N_y \times N_z = 100 \times 51 \times 51 = 260,100$) with $g = 1$, which gives a cell size of about 8.2 mm on the boundaries AB and CD, and a cell size of about 21.7 mm on the boundaries AD and BC. The mesh in the domain Ω_1 has 57,500 cells ($=N_x \times N_r \times N_\theta = 100 \times 115 \times 50 = 575,000$) with $g = 1.1$, which gives the distance between S_B and S_{F1} (along any one of the rays) as $l = 52$ mm with the size of the cell adjacent to S_{F1} as 4.3 mm and in the circumferential direction an angle of 7.2 deg. The length of wall adjacent cell (l_1) is 0.001 mm. The discretization of the domains Ω and Ω_1 are shown in **Figure 6** for the toy submarine.

The comparison of the drag forces obtained using CFD as reported by Alam *et al.* (2015) with present CFD calculations are recorded in **Table 4** showing very good match (within 0.2% difference). The drag values obtained by Eqns. (2.3), (2.4) and (2.5) were reported by Alam



(a)



(b)

Figure 6. Mesh for toy submarine USS Dallas (No. of nodes 835,100; no. of cells 956,664). (a) Mesh in the full domain for toy submarine USS Dallas. (b) Mesh in the Ω_1 for toy submarine USS Dallas.

Source	D (N)
CFD (Alam <i>et al.</i> (2015) (realizable $k-\epsilon$ model)	0.1065
CFD (Present) (SST $k-\omega$ model)	0.1062
Difference (%)	-0.2

Table 4. Comparison of drag forces of toy submarine USS Dallas at $U = 0.5$ m/s ($Re_L = 1.75 \times 10^5$).

et al. (2015). The mesh convergence study is not reported here because the present mesh with about 1 million cells is much finer than 0.69 million cells used in Alam *et al.* (2015).

4.1. CFD analysis of AUV Cormoran

The mesh of the domain Ω (see **Figure 5**) for AUV Cormoran has 26,010 cells ($= N_x \times N_y \times N_z = 100 \times 51 \times 51 = 260,100$) with $g = 1$, which gives a cell size of about 33 mm on the boundaries AB and CD, and a cell size of about 92.3 mm on the boundaries AD and BC. The mesh in the domain Ω_1 has 575,000 cells ($= N_x \times N_r \times N_\theta = 100 \times 115 \times 50 = 575,000$) with $g = 1.1$, which gives the distance between S_B and S_{F1} (along any one of the rays) as $l = 52$ mm with the size of the cell adjacent to S_{F1} as 4.3 mm and in the circumferential direction an angle of 7.2 deg. The length of wall adjacent cell (l_1) is 0.001 mm. The discretization of the domains Ω and Ω_1 are shown in **Figure 7**.

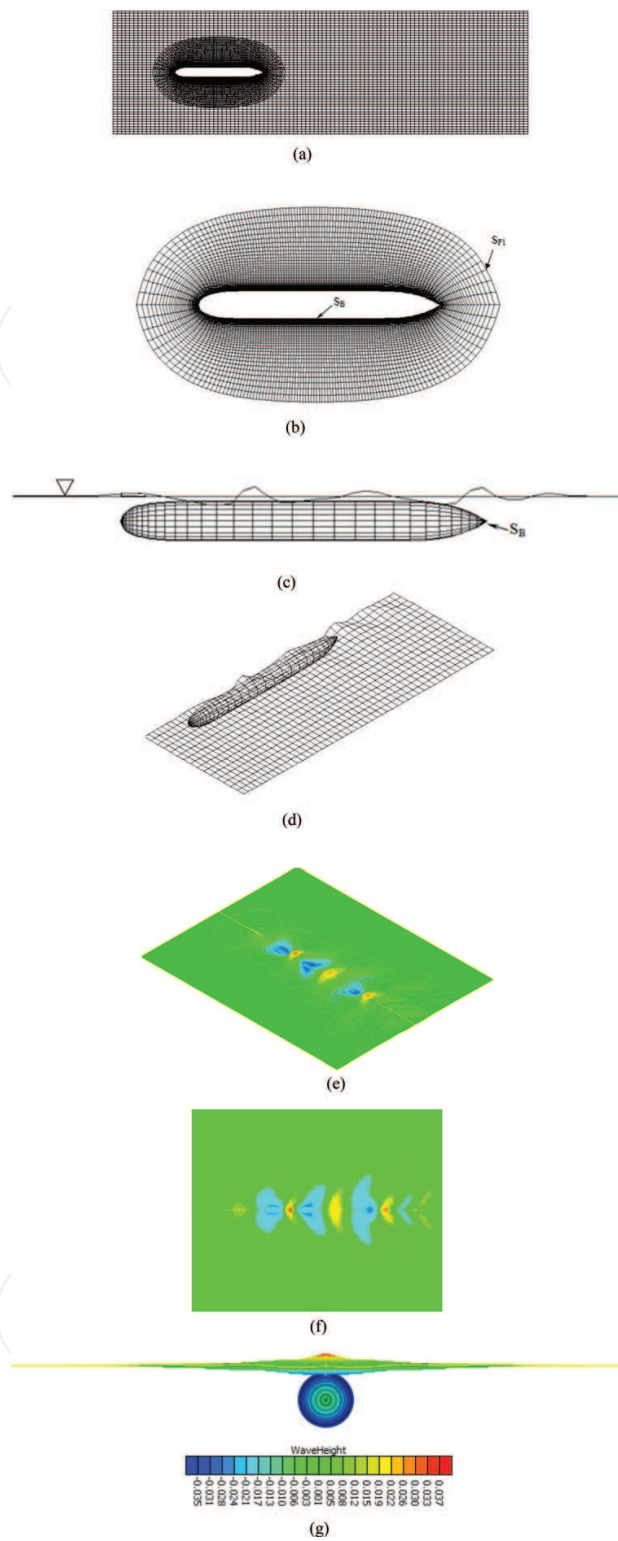


Figure 7. Mesh for AUV Cormoran. (a) Mesh in the full domain for AUV Cormoran(No. of nodes 835,100; no. of cells 956,664). (b) Mesh in the Ω_1 for AUV Cormoran (c) panels on AUV Cormoran. (d) Panels on AUV Cormoran and free surface (one half shown) (No. of panels = 3500 on S_B , = 1500 on free surface, = 5000 total). (e) Surface wave pattern generated by AUV Cormoran ($U = 1$ m/s). (f) Surface wave pattern generated by AUV Cormoran in top view ($U = 1$ m/s). (g) Surface wave pattern generated by AUV Cormoran in front view ($U = 1$ m/s).

(a) Comparison with experiments				
U (m/s)	C_D	C_W	$C_T = C_D + C_W$	
	CFD (Present)		CFD (Present)	Experimental (Alvarez <i>et al.</i> [2008])
0.916	0.004524	0.004524	0.009048	0.00913
1.062	0.004463	0.004866	0.00932	0.00989
1.195	0.004325	0.007827	0.0121	0.01291
1.399	0.004222	0.003998	0.00822	0.00871
(b) Comparison with empirical formulae				
U (m/s)	C_D			
	CFD			
0.916	0.004524	0.0047	0.004692	0.004729
1.062	0.004463	0.004555	0.00455	0.004585
1.195	0.004325	0.00445	0.00444	0.004474
1.399	0.004222	0.004309	0.0043	0.004333

C_W coefficient of wave resistance.

Table 5. Comparison of drag coefficients of AUV Cormoran.

The experimental drag forces as reported by Alvarez *et al.* (2008) are for snorkeling depth of submergence ($z = -0.05$ m, see **Figure 5**) which will induce wave making drag in addition to viscous drag. In order to capture the wave-making component of drag, a free surface boundary condition is specified on the boundary AD (see **Figure 5** and **7b**). The dimensions of the free surface are $2L$ in the x -direction and L in the y -direction. The surface is discretized with 50 equispaced panels in the x -direction, which gives a panel size of 28.4 mm and with 30 equispaced panels in the y -direction, which gives a panel size of 35.5 mm, making a total of 1500 panels. On the surface S_B , in the x -direction, for $0 \leq x \leq L_n$ number of panels are 40 with a $g = 1.1$, in between $L_n \leq x \leq L_n + L_m$, 10 with $g = 1$ and between $L_n + L_m \leq x \leq L$, 20 with $g = 1.1$ making a total of 70 panels and in the circumferential direction, 50 equispaced panels, each making an angle of 7.2 deg. The surface wave pattern generated by AUV Cormoran for $U = 1$ m/s is shown in **Figures 7(e), 7(f)** and **7(g)**.

The comparisons of the drag forces are recorded in **Table 5** for four forward speeds. As can be seen, the present calculations are very accurate.

5. Conclusion

A critical review of the literature brings out the following: Several AUV, AUG, submarine and similar vehicle shapes had been treated using the CFD approach. A nearly exhaustive list of these shapes are: Afterbody 1, Afterbody 2, modified spheroid and F57, AUV Rainbow, AUV Cormoran, AUV Autosub and AUV Soton, AUG Alex, AUV PICASSO, AUV Petrel, AUG USM, AUV

Flinders, toy submarine USS Dallas and AUG Seawing. From the literature, it is observed that the use of CFD in the hydrodynamic design of UVs is finding increasing acceptance, as is evident by the fact that about 15 UV shapes have been treated. The CFD methodology adopted in the present work has been validated with a few example problems from the literature. The hydrodynamic parameters computed by CFD are drag and wave resistance.

Author details

Kondeti Lakshmi Vasudev

Address all correspondence to: kondetilv@hindustanuniv.ac.in

Department of Mechanical Engineering, Hindustan Institute of Technology and Science, Chennai, India

References

- [1] Parsons JS, Goodson RE, Goldschmied FR. Shaping of axisymmetric bodies for minimum drag in incompressible flow. *Journal of Hydronautics*. 1974;8(3):100-107
- [2] <http://www.navaldrones.com/SPURV.html>
- [3] <http://auvac.org/configurations/view/135>
- [4] http://auvlab.mit.edu/MURI/1997_Rprtfinal.html
- [5] <http://www.whoi.edu/page.do?pid=83577&tid=3622&ci>
- [6] <http://www.geojetimes.co.kr/news/articleView.html?idxno=25928>
- [7] <http://www.nauticexpo.com/prod/mitsubishi-heavy-industries-ship-ocean>
- [8] <http://www.act-us.info>
- [9] <http://www.ise.bc.ca/theseus.html>
- [10] <http://www.unmanned.co.uk/platforms/unmanned-vehicles-news/page/108/>
- [11] http://www.act-us.info/sensor_list.php?cat=AUV&type=Sensor%20Type
- [12] <http://www.km.kongsberg.com/ks/web/nokbg0240.nsf/AllWeb/EC2FF8B58CA491A4C1257B870048C78C?OpenDocument>
- [13] http://www.nio.org/index/option/com_newsdisplay/task/view/tid/4/sid/23/nid/88
- [14] Alam K, Ray T, Anavatti SG. A new robust design optimization approach for unmanned underwater vehicle design. *Journal of Engineering for the Maritime Environment*. 2012; 226(3):235-249

- [15] Campana EF, Peri D, Tahara Y, Stern F. Shape optimization in ship hydrodynamics using computational fluid dynamics. *Computer Methods in Applied Mechanics and Engineering*. 2006;**196**(1-3):634-651
- [16] Shahid M, Huang D. Computational fluid dynamics based bulbous bow optimization using a genetic algorithm. *Journal of Marine Science and Applications*. 2012;**11**:286-294
- [17] Gertler M. Resistance experiments on a systematic series of streamlined bodies of revolution—For application to the design of high-speed submarines. In: DTRC Report: C-849. Washington, D.C; 1950
- [18] Patel VC, Nakayama A, Damain R. Measurements in the thick axisymmetric boundary layer near the tail of a body of revolution. *Journal of Fluid Mechanics*. 1974;**63**(2):345-367
- [19] Ray T, Gokarn RP, Sha OP. A global optimization model for ship design. *Computers in Industry*. 1995;**26**:175-192
- [20] Alexandrov N, Dennis JE Jr, Lewis RM, Torczon V. A trust region framework for managing the use of approximation models in optimization. *Structural Optimization*. 1998;**15**(1): 16-23
- [21] Percival S, Hendrix D, Noblesse F. Hydrodynamic optimization of ship hull forms. *Applied Ocean research*. 2001;**23**(6):337-355
- [22] Peri D, Campana EF. High fidelity models and multi-objective global optimization algorithms. *Journal of Ship Research*. 2005;**49**(3):159-175
- [23] Tahara Y, Tohyama S, Katsui T. CFD based multi-objective optimization method for ship design. *International Journal for Numerical Methods in Fluids*. 2006;**52**:499-527
- [24] Demko D. Tools for Multi-Objective and Multi-Disciplinary Optimization in Naval Ship Design [Thesis]. Virginia Polytechnic Institute and State University; 2006

